Experimental Validation of Multi-vehicle Coordination Strategies

J. A. Marshall, T. Fung, M. E. Broucke, G. M. T. D'Eleuterio, and B. A. Francis

Abstract— **Consequent to previously published theoretical work by Marshall, Broucke, and Francis, this paper summarizes the apparatus and results of multi-vehicle coordination experiments conducted at the University of Toronto Institute for Aerospace Studies. These experiments successfully demonstrated the practicality of cyclic pursuit as a distributed control strategy for multiple wheeled-vehicle systems. Moreover, the pursuit-based coordination algorithm was found to be surprisingly robust in the presence of unmodelled dynamics and delays due to sensing and information processing.**

I. Introduction

In [1], [2], Marshall et al. introduced the notion of *pursuit* as a technique for coordinating the motions of multiple wheeled-vehicles in the plane. More specifically, *cyclic pursuit* was studied in a purely theoretical way as a means for achieving certain regular geometric formations for a system of identical kinematic unicycles. This approach is particularly simple in that the n vehicles are ordered such that vehicle i pursues vehicle $i+1$, modulo n.

The current research on pursuit strategies for multi-vehicle systems is partially motivated by the prevalence of similar distributed control algorithms found in nature [3], [4]. Moreover, this type of formation strategy might have potential application in the deployment of distributed sensor arrays, enabling scientists to collect simultaneous seismological, meteorological, or other pertinent environmental data on planetary exploration missions [5].

A. Theoretical Background

Consider a system of n vehicles in the plane, each modelled as a kinematic unicycle with nonlinear state model

$$\begin{bmatrix} \dot{x}_i \\ \dot{y}_i \\ \dot{\theta}_i \end{bmatrix} = \begin{bmatrix} \cos\theta_i & 0 \\ \sin\theta_i & 0 \\ 0 & 1 \end{bmatrix} \begin{bmatrix} v_i \\ \omega_i \end{bmatrix}, \qquad (1)$$

for $i = 1, 2, \ldots, n$ and where $[x_i, y_i]^\top \in \mathbb{R}^2$ is the i-th vehicle's position, $\theta_i \in \mathbb{S}^1$ is its orientation, and where $[v_i, \omega_i]^\top \in \mathbb{R}^2$ are control inputs. Let α_i denote the difference between the i-th vehicle's heading and the heading that would take it directly towards its target, $i+1$ (as in Fig. 1). An intuitive pursuit law for (1) is to assign vehicle i's angular speed ω_i in proportion to the heading error, α_i. Following [2], we consider the case when the vehicles move with the same fixed forward speed, v_R. In particular, we are interested in the distributed control law

$$v_i = v_R \text{ and } \omega_i = k_\alpha \alpha_i, \qquad (2)$$

where $k_\alpha > 0$ is constant. Simulation and analysis results have shown that asymptotically stable circular pursuit trajectories are achievable, as illustrated for $n = 3$ in the simulation of Fig. 2. The relative coordinates $[r_i, \alpha_i, \beta_i]^\top$ of Fig. 1 prove useful, since in steady state these variables become constant. Let $z_i \in \mathbb{R}^2$, $i = 1, 2, \ldots, n$, and consider the following definition from geometry.

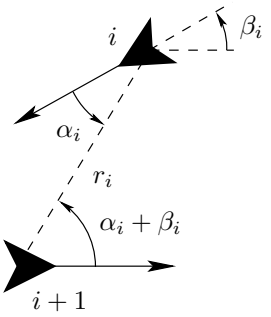

Fig. 1. Relative coordinates, with vehicle i in pursuit of $i+1$.

Definition 1 (after [6], p. 93): Let n and $d < n$ be positive integers so that $p := n/d > 1$ is a rational number. Let R be the positive rotation in the plane, about the origin, through angle $2\pi/p$ and let $z_1 \neq 0$ be a point in the plane. Then, the points $z_{i+1} = Rz_i$, $i = 1, 2, \ldots, n-1$ and edges $e_i = z_{i+1} - z_i$, $i = 1, 2, \ldots, n$, define a *generalized regular polygon*, which is denoted $\{p\}$.

For example, the vehicles in Fig. 2 converge to a $\{3/1\}$ generalized regular polygon formation. Indeed, in [2] it was revealed that, subject to the inputs (2), certain generalized regular polygon formations are locally asymptotically stable, while others are not. Table I lists all possible equilibrium polygon formations and gives their stability.

B. Experimental Purpose

Over the past several years, a number of so-called *Argo Rovers* (the allusion being to the Greek myth of Jason, the Argonauts and the Golden Fleece, since names belonging to the Argonauts have been bestowed on rovers of the fleet) have been constructed at the Space Robotics Laboratory of the University of Toronto Institute for Aerospace Studies (UTIAS). The robots were designed to be capable of lengthy autonomous operation and have each been equipped with a host of sensing, communication, and actuation devices. For more specific details, see [7].

This work was supported in part by the Natural Sciences and Engineering Research Council of Canada (NSERC) and the Centre for Earth and Space Technology (CRESTech).

J. A. Marshall, T. Fung, M. E. Broucke, and B. A. Francis are with the Systems Control Group of the Department of Electrical and Computer Engineering, University of Toronto, 10 King's College Rd, Toronto, ON M5S 3G4, Canada joshua.marshall@utoronto.ca

G. M. T. D'Eleuterio is with the Space Robotics Group of the University of Toronto Institute for Aerospace Studies, 4925 Dufferin St, Toronto, ON M3H 5T6, Canada gabriele.deleuterio@utoronto.ca

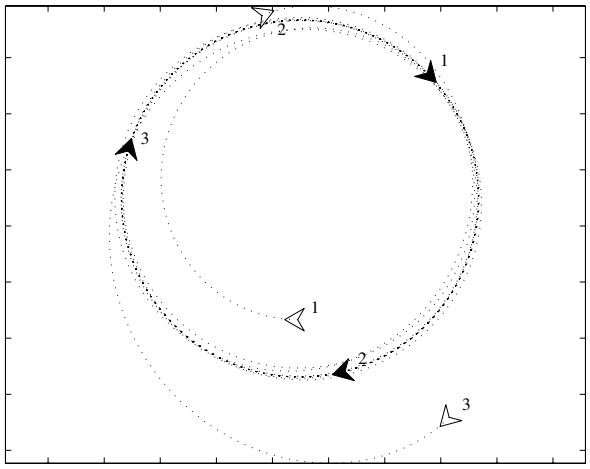

Fig. 2. Three unicycles subject to control law (2), with $k_\alpha = 0.6$.

TABLE I
EQUILIBRIUM POLYGONS WITH STABLE POLYGONS SHADED [2].

$d=1$	2	3	4	5	6
{2/1}	{3/2}	{4/3}	{5/4}	{6/5}	{7/6}
{3/1}	{4/2}	{5/3}	{6/4}	{7/5}	{8/6}
⋮	⋮	⋮	⋮	⋮	⋮
{7/1}	{8/2}	{9/3}	{10/4}	{11/5}	{12/6}
{8/1}	{9/2}	{10/3}	{11/4}	{12/5}	{13/6}
⋮	⋮	⋮	⋮	⋮	⋮
{17/1}	{18/2}	{19/3}	{20/4}	{21/5}	{22/6}
{18/1}	{19/2}	{20/3}	{21/4}	{22/5}	{23/6}
⋮	⋮	⋮	⋮	⋮	⋮
{49/1}	{50/2}	{51/3}	{52/4}	{53/5}	{54/6}
{50/1}	{51/2}	{52/3}	{53/4}	{54/5}	{55/6}
⋮	⋮	⋮	⋮	⋮	⋮

Since the theoretical results summarized in subsection I-A were based on ideal kinematic unicycles, one might naturally question whether the intuitive control law (2) has more general applicability (e.g., to real vehicles, possessing non-trivial dynamics, such as the Argo Rovers). Also, despite the growing amount of theoretical research on cooperative control strategies employing local interaction-based techniques, there are relatively few instances of experimental research validating their worth. Therefore, the purpose of our experiments is twofold:

i. to determine if the theoretical results of [2], obtained for kinematic unicycles, could be observed in practise using the four-wheeled Argo Rovers;
ii. to investigate the practicality of (2) as a multi-vehicle coordination strategy given real hardware restrictions (e.g., processing delays, sensor limitations).

A brief description of our experimental procedure, a detailed summary of the results, and a discussion of our observations and their significance follow.

C. Overview of the Rovers

Built using the Tamiya TXT-1 4×4 Pick-up chassis, the Argo Rovers were designed to be fully autonomous mobile robots suitable for outdoor use.

1) Microelectronics, Software, and Communications: Each rover possesses a 700 MHz Pentium® III processor-based computer with a 1 GB micro-drive, 256 MB of RAM, two PCMCIA slots, two USB ports, and runs the Debian-Linux operating system. C/C++ language software interfaces with onboard sensors and actuators by way of a Siemens C164 20 MHz 16-bit microcontroller (for processing low-level hardware routines). Each is fitted with a wireless Ethernet card used for remote software development, operation, and for communication between rovers.

2) Power Systems: To conserve payload space and to lower the rover's center of gravity, each rover is powered by 1.2 V NiMH batteries, ten of which are located (in series) inside each rubber tire. Current is subsequently delivered to the individual rover systems by way of a custom designed circular slip-ring on each wheel hub.

3) Motion Actuators and Encoders: Front and rear wheel steering axis angles are adjustable independently via servomotor driven mechanisms at each axis. Moreover, each rover is propelled at all four wheels by a geared throttle motor. The rovers can travel at speeds of not much more than 0.5 m/s with a minimum turning radius of approximately 0.65 m. Each is equipped with a rotary optical encoder (512 cycles per shaft turn) in the hub of each wheel.

4) Camera-based Vision Systems: Each rover is equipped with two CCD array video cameras capable of acquiring up to 640×480 pixel resolution images at a frequency of 30 Hz. Furthermore, each camera is fixed to a stereovision head using custom supports that allow for individual pan and tilt by way of servomotor mechanisms.

II. DESIGN AND IMPLEMENTATION

This section briefly describes the hardware and software engineering designs used to fulfil the experimental purpose discussed in subsection I-B.

A. Rover Dynamics

As a design tool and, perhaps more importantly, to illustrate how significantly different the rovers are from kinematic unicycles, we first develop a simple model of the rover dynamics. Owing to limited workspace in the laboratory, for our experiments the rovers were operated with their front and rear wheel axes *locked* for tightest turning. Therefore, let ϕ denote the steering angle, as illustrated in the body-centered-axis model of Fig. 3, so that the rover's configuration can be described by the state variables $[x, y, \theta, \phi]^\top$. The half-length $l \approx 0.3$ m. Let $m \approx 15$ kg denote the rover's mass, I_p its body moment of inertia about the point (x, y), and I_s the effective inertia that needs to be overcome by the steering actuator. If we ignore

any frictional effects, it can be shown that the resulting equations of motion are

$$\dot{x} = v_f \cos\phi \cos\theta \tag{3a}$$
$$\dot{y} = v_f \cos\phi \sin\theta \tag{3b}$$
$$\dot{\theta} = v_f \tfrac{1}{l} \sin\phi \tag{3c}$$
$$\dot{\phi} = \omega_\phi \tag{3d}$$
$$\dot{v}_f = \left(m\cos^2\phi + \tfrac{1}{l^2} I_p \sin^2\phi\right)^{-1} \times \left[v_f \omega_\phi (m - \tfrac{1}{l^2} I_p)\cos\phi\sin\phi + f\right] \tag{3e}$$
$$\dot{\omega}_\phi = \tau / I_s, \tag{3f}$$

where v_f is the forward velocity in the direction of the wheels, f is the throttle force input acting in the direction of the wheels, and τ is the steering torque input.

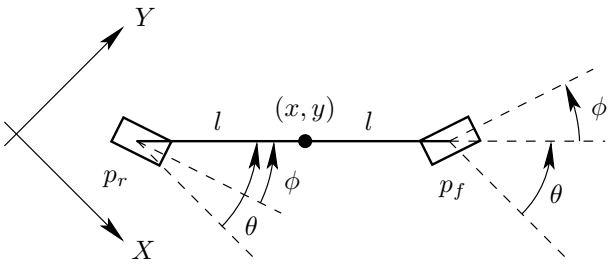

Fig. 3. Rover body-centered-axis model with wheel-axes locked.

B. Speed Regulation

To approximate the control law (2), it was necessary to equalize the rover speeds. Therefore, a basic speed regulator was designed for each rover using feedback from its four wheel encoders. The actual rolling speed v_f was estimated by numerically differentiating position data acquired from the encoders every $T = 0.1$ s (or 10 Hz). The estimated wheel-speeds were averaged to generate $\hat{v}_f(kT)$, $k = 0, 1, 2, \ldots$, at each time step. Because of significant noise in the speed estimates, the differentiated encoder data was low-pass filtered (-3 dB at 1.35 Hz).

Based on our knowledge of the model in subsection II-A, a PI compensator was implemented digitally using finite-difference approximations and the estimated speed error $e_v(kT) := v_R - \hat{v}_f(kT)$. Thus, for the servomotor input command $u_v \in [-1, 1]$, the employed discrete-time PI controller was $u_v(kT) = k_P e_v(kT) + u_I(kT)$, where

$$u_I(kT) = u_I(kT - T) + k_I \frac{T}{2}\left[e_v(kT) + e_v(kT - T)\right],$$

with $u_I(0) = 0$. Through online tuning experiments, gains of $k_P = 1.5$ and $k_I = 2.5$ were found to work well. An example of the speed regulator response is provided in Fig. 4, as estimated using encoder data. Due to particularities of the transmission (significant play), of the chassis (significant sway), and of the wheels (placement of the batteries), small fluctuations in speed were always present and could be audibly discerned while the rovers were running, even during open-loop driving.

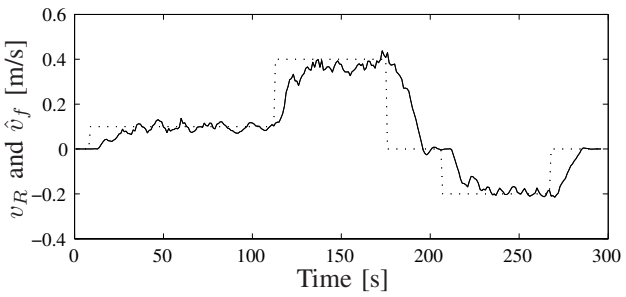

Fig. 4. Example speed regulator response with changing reference speeds.

C. Multi-vehicle Pursuit using Vision

As described in subsection I-C.3, each rover's steering angle ϕ is *directly* specifiable by way of its steering servomotors, thus the torque input τ of (3f) is not actually an available input. Therefore, the actual steering mechanism dynamics were ignored and ϕ was itself computed so as to emulate $\dot{\theta} = k_\alpha \alpha$. In other words, using (3c), one obtains

$$v_{f_i}(kT) = v_R \text{ and } \phi_i(kT) = \arcsin\left[\frac{l k_\alpha \alpha_i(kT)}{v_R}\right], \tag{4}$$

for $i = 1, 2, \ldots, n$, as an intuitive cyclic pursuit law for multiple rovers, which mimics (2).

The right camera on each rover was used to acquire 160×120 pixel (low resolution) images, which were then used to estimate the heading error $\alpha(kT)$. The rovers were each suited with a cylinder of different colored cardboard so that ordering of the vehicles could be accomplished by simply ordering the colors. Target localization was done by scanning the pixels in an acquired image and comparing each pixel's hue value with a preset nominal target value. Those pixels within a specified tolerance of the nominal were recorded and their horizontal positions averaged to compute an estimate of the target's location in the image. Using knowledge of the camera's focal length and orientation, the angle $\alpha(kT)$ was easily estimated.

Because the horizontal field-of-view (FOV) of the on-board cameras is relatively low (approximately 34 degrees), in our initial experiments the rovers lost track of their targets very easily. To augment the FOV, its panning servomotor was employed, increasing the FOV to approximately 150 degrees. This was done by using the computed target location as feedback for actuation of the camera's panning servomechanism (by way of another PI compensator) so as to actively center the target in the camera's image plane.

III. Experiments and Observations

A variety of experiments were conducted using groups of two, three, and four rovers. Despite the significant physical differences between ideal kinematic unicycles and the Argo Rover systems (a natural conclusion of the previous section) the outcome was surprisingly positive.

Our first experiments were done using two rovers. In this case, the only theoretically possible formation is the $\{2/1\}$ polygon (i.e., two vehicles diametrically opposite each other

on a circular path). We found that, so long as no rover lost the other from its view, the vehicles always converged to a $\{2/1\}$-polygon formation.

A. *Stability of the* $\{3/1\}$*-polygon Formation*

In theory, the possible equilibrium formations for three vehicles are the $\{3/1\}$ and $\{3/2\}$ polygons. Although both resemble equilateral triangles, it is the vehicles' ordering on the circle circumscribed by each polygon that is different. As per Definition 1, a $\{3/1\}$ formation corresponds to the case when the i-th vehicle's target, $i+1$, lies at a heading error of $\alpha_i = \pm\pi/3$. Conversely, a $\{3/2\}$ formation corresponds to $\alpha_i = \pm 2\pi/3$. According to Table I, of the two possible equilibria only the $\{3/1\}$-polygon formation is locally asymptotically stable.

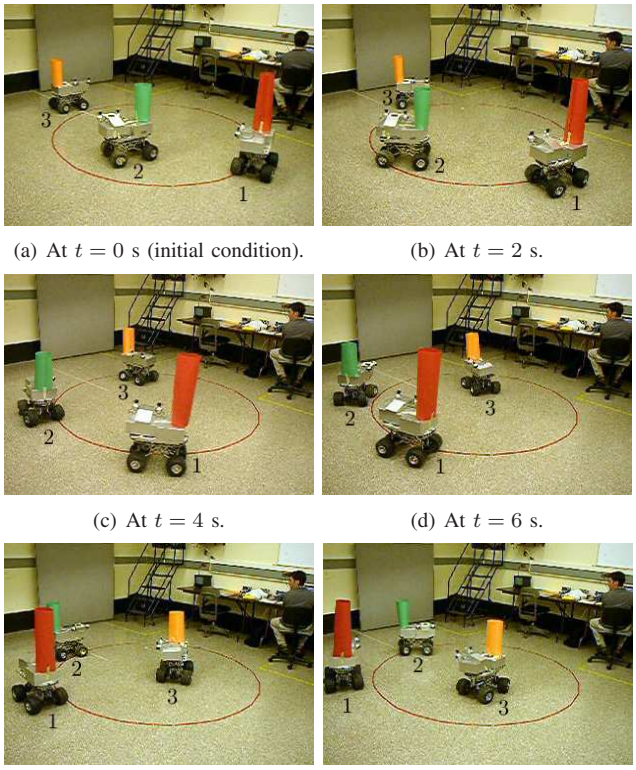

(a) At $t = 0$ s (initial condition). (b) At $t = 2$ s.

(c) At $t = 4$ s. (d) At $t = 6$ s.

(e) At $t = 8$ s. (f) At $t = 10$ s.

Fig. 5. Generating a $\{3/1\}$ formation with $k_\alpha = 0.2$.

As previously noted, Fig. 2 shows three unit-speed unicycles, subject to (2), converging to a $\{3/1\}$ formation (the simulation ends after 45 s). On the other hand, Fig. 5 presents a sequence of images captured of three Argo Rovers in cyclic pursuit, subject to (4). Fig. 6 shows the heading errors, α_i, $i = 1, 2, 3$, as a function of time for each of the simulated unicycles in Fig. 2 (dotted lines) and for the actual rovers of Fig. 5 (solid lines). The time axis in Fig. 6 corresponds almost exactly to the times noted for each image frame in Fig. 5. The actual rover heading errors were recorded only every second, although they were computed every 0.1 s. Clearly, owing to their physical differences, the unicycle and rover trajectories should not be expected to match in the transient. However, Fig. 6 shows that their steady-state behaviors both tend to equally spaced motion around a stationary circle of fixed radius. Convergence of the real rovers to a stable $\{3/1\}$ formation, with $\alpha_i = -\pi/3$, is clear from Fig. 5.

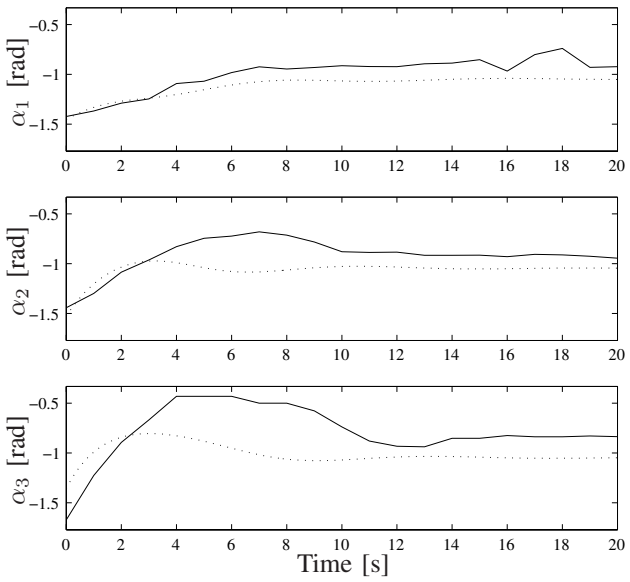

Fig. 6. Kinematic unicycle (dotted lines, cf. Fig. 2) together with actual rover (solid lines, cf. Fig. 5) target heading errors. In both cases, the errors converge to approximately $\alpha_i = -\pi/3$.

Additional experiments were performed where the rovers were first allowed to achieve a steady-state $\{3/1\}$ formation. Subsequently, one of the rovers was deliberately perturbed from this equilibrium by either altering its heading, halting it temporarily, or slightly changing its location. So long as the rovers were able to maintain their targets within view, the group always returned to a $\{3/1\}$-polygon configuration, further demonstrating its stability as a formation.

B. *Formation Radius and the* $\{4/1\}$*-polygon*

Results equivalent to those described above for the $\{3/1\}$ formation were also found using four vehicles. Fig. 7 shows four rovers maintaining a $\{4/1\}$-polygon formation.

Furthermore, in [2] it was proved that the kinematic unicycles traverse a circle of radius $\rho = v_R n/k_\alpha \pi d$ at equilibrium, where $\{n/d\}$ is the formation. Therefore, by increasing (resp. decreasing) the gain k_α we should have expected to observe a proportional decrease (resp. increase) in the radius traversed by the rovers, which was indeed the case. Fig. 7 shows four rovers in cyclic pursuit, each with gain $k_\alpha = 0.3$, after having stabilized to a $\{4/1\}$-polygon configuration. At approximately $t = 7$ s, the gain k_α was decreased from 0.3 to 0.1 on all the rovers. The sequence of images shows how the rovers continued to maintain a $\{4/1\}$ formation while, at the same time, the polygon's radius effectively tripled in size. Identical results were also observed for groups of two and three rovers.

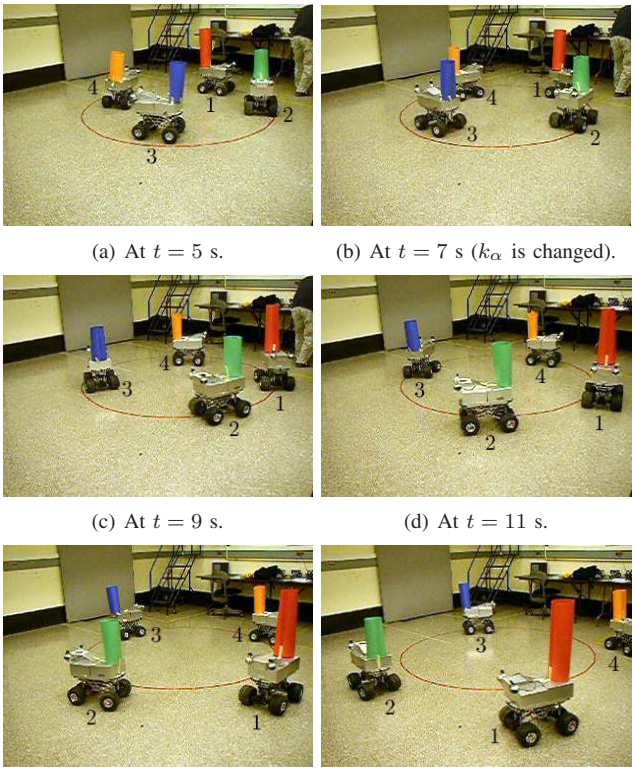

(a) At $t = 5$ s. (b) At $t = 7$ s (k_α is changed).

(c) At $t = 9$ s. (d) At $t = 11$ s.

(e) At $t = 13$ s. (f) At $t = 15$ s.

Fig. 7. A $\{4/1\}$ formation after k_α is changed from 0.3 to 0.1.

C. The $\{3/2\}$-polygon Formation

Although, in theory, the $\{3/2\}$ formation for unicycles is unstable (see Table I), computer simulations suggest that it is not so unstable that, while maintaining the ordering of vehicles, *almost*-circular trajectories are not achievable for a lengthy time period. Fig. 8a shows a simulation of three unit-speed unicycles that start roughly in the $\{3/2\}$ configuration (the simulation ends after 45 s). Despite the fact that they do not converge to a $\{3/2\}$ polygon, their motion appears to maintain an *almost*-$\{3/2\}$ formation. Interestingly, among the six important eigenvalues associated with the system's linearization about the $\{3/2\}$ polygon (in relative coordinates; see [2] for details), there is only one complex-conjugate pair of unstable eigenvalues and these eigenvalues lie particularly close to the imaginary axis ($\lambda \approx 0.0419 \pm j1.5303$). If the simulation of Fig. 8a is continued for more than 250 s, the unicycles eventually break their pattern of motion and rearrange themselves into a stable $\{3/1\}$ formation, as illustrated by Fig. 8b.

Fig. 9 presents a sequence of images captured of three rovers in cyclic pursuit (using the same pursuit order as the rovers in Fig. 5). Both the unicycles of Fig. 8 and the rovers of Fig. 9 started close to a $\{3/2\}$ formation. Consequently, their resulting trajectories appear *qualitatively* similar, maintaining the ordering of a $\{3/2\}$ polygon yet never actually converging to a stable formation. If allowed to run for long enough, the rover formation was also seen

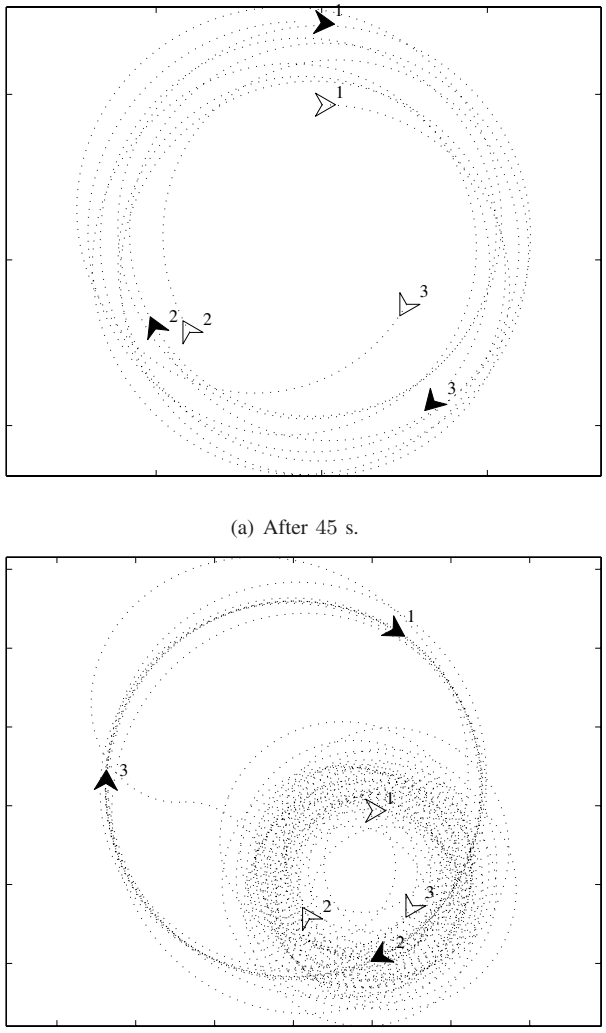

(a) After 45 s.

(b) After 300 s.

Fig. 8. Unicycles demonstrating a $\{3/2\}$ almost-stable formation with $k_\alpha = 0.2$. The initial conditions are the same for both (a) and (b).

to "wobble," as in Fig. 8a. However, even after several minutes, evolution of the rovers into a $\{3/1\}$-polygon formation was never observed[1], unlike what happens in simulation for unicycles (cf. Fig. 8b). Nevertheless, it is clear from Fig. 9 that the $\{3/2\}$ polygon is not asymptotically stable for rovers, as predicted by the theory for unicycles.

Similar to Fig. 6, in Fig. 10 the heading errors α_i, $i = 1, 2, 3$, have been plotted as a function of time for each of the simulated unicycles in Fig. 8 (dotted lines) and for the actual rovers of Fig. 9. The time axis in Fig. 10 corresponds almost exactly to the times noted for each image frame in Fig. 9. Again, owing to their physical differences, the unicycle and rover trajectories should not be expected to match. However, Fig. 10 shows how their behaviors are

[1]On the other hand, this type of maneuver was likely not even possible given the limited field-of-view of the cameras and the fact that we did not implement a protocol for collision avoidance among rovers.

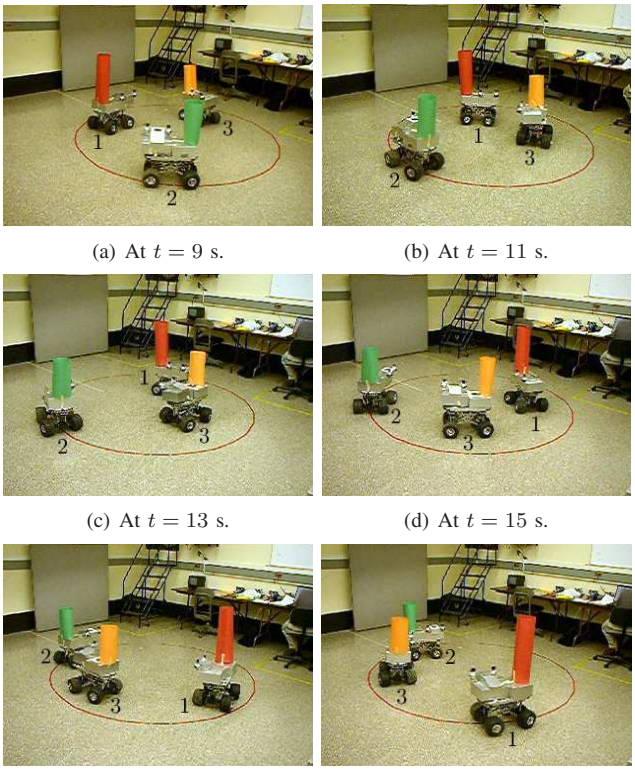

(a) At $t = 9$ s. (b) At $t = 11$ s.

(c) At $t = 13$ s. (d) At $t = 15$ s.

(e) At $t = 17$ s. (f) At $t = 19$ s.

Fig. 9. A $\{3/2\}$ semi-stable formation with $k_\alpha = 0.1$.

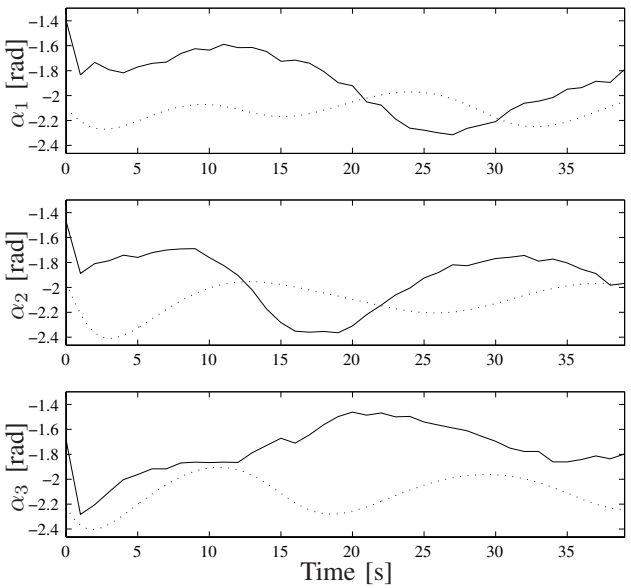

Fig. 10. Kinematic unicycle (cf. Fig. 8a, dotted lines) together with actual rover (cf. Fig. 9, solid lines) heading errors. Note how their behaviors are qualitatively consistent in that similar oscillations appear in both cases.

qualitatively the same, with oscillations appearing in the heading errors of both the unicycles and the rovers.

IV. Summary and Conclusions

Given the physical differences between kinematic unicycles and the Argo Rovers, and that there were delays in the system due to sensing and information processing not accounted for in the accompanying theory [2], the presented experimental results are very encouraging.

However, success is not to say there were not limitations. Firstly, owing to the difficulties in bringing multiple rovers into working order (i.e., free of hardware difficulties), experiments were limited to $n = 4$ rovers. Although it is likely that the reported results extend to $n > 4$ rovers, no experiments were conducted to confirm this. Secondly, the rovers were severely limited by the field-of-view of their cameras. Even with the inclusion of camera servoing, for certain initial conditions the rovers inevitably lost their target, thus limiting the range of experiments that could be tried. On the other hand, computation of the control law was based solely on sensing and data processing carried out *locally* (i.e., without any explicit communication, nor the use of an overhead camera system or other GPS). Finally, experiments were further restricted by the fact that no method of collision avoidance was employed, an important practical issue not considered in this research.

In conclusion, the relatively simple cyclic pursuit strategy developed for unicycles in [2] was found to be practical from the point-of-view of robustness to unmodelled dynamics, disturbances in the vehicle velocities, and delays in the system due to sensing and information processing. These findings not only bode well for continuing research on cooperative control strategies based on the notion of pursuit, but also for other cooperative control techniques employing similar local interactions.

V. Acknowledgements

Thanks to M. A. Mirza and A. M. Rotenstein for helpful discussions regarding the vision systems, and R. Yachoua for logistical help and for taking video. Most of the utilized Linux I/O code was written by L. Ng and the C164 microcontroller was originally programmed by E. J. P. Earon.

References

[1] J. A. Marshall, M. E. Broucke, and B. A. Francis, "A pursuit strategy for wheeled-vehicle formations," in *Proceedings of the 42nd IEEE Conference on Decision and Control*, Maui, Hawaii, December 2003, pp. 2555–2560.

[2] ——, "Formations of vehicles in cyclic pursuit," *IEEE Transactions on Automatic Control*, vol. 49, no. 11, pp. 1963–1974, November 2004.

[3] J. K. Parrish, S. V. Viscido, and D. Grünbaum, "Self-organized fish schools: An examination of emergent properties," *Biological Bulletin*, vol. 202, pp. 296–305, June 2002.

[4] C. W. Reynolds, "Flocks, herds, and schools: A distributed behavioural model," *Computer Graphics*, vol. 21, no. 4, pp. 25–34, July 1987.

[5] T. D. Barfoot, E. J. P. Earon, and G. M. T. D'Eleuterio, "Controlling the masses: Control concepts for multi-agent mobile robotics," in *Second Canadian Space Exploration Workshop*, Calgary, Canada, October 1999.

[6] H. S. M. Coxeter, *Regular Polytopes*. London: Methuen & Co. Ltd., 1948.

[7] M. A. Mirza, D. M. Beach, E. J. P. Earon, and G. M. T. D'Eleuterio, "Development of a next-generation autonomous robotic network and experimental testbed," in *Proceedings of the Planetary and Terrestrial Mining Sciences Symposium*, Sudbury, Canada, June 2004.